Numerical Modelling-Based Methodology for Generating Fragility Curves of Underground Tunnels under Static Loading

Shahriyar Heidarzadeh
SNC-Lavalin, Montreal, Canada

Ali Saeidi
Université du Québec à Chicoutimi, Chicoutimi, Canada

ABSTRACT: We present a method to assess the robustness of underground tunnels against brittle failure by creating vulnerability functions based on rock mass quality and static loading intensities. Using a Monte Carlo Simulation and FLAC3D, we simulated multiple models of a tunnel in rock masses with varying qualities and subjected to different static loads. Fragility curves were constructed using a stress-based failure criterion to measure the severity of brittle damage. Mathematical approximations were used to generate vulnerability functions linking occurrence probabilities of damage states to loading intensities. Results showed that fragility curves offer a numerically developed tool for design engineers to predict different damage states based on variations in rock mass quality and in situ stress state.

Keywords: Fragility curves, underground tunnels, vulnerability functions, brittle damage, FLAC3D.

1 INTRODUCTION

To ensure the stability of underground excavations, it is important to assess the potential for damage or failure. This assessment, known as fragility assessment, determines the likelihood of damage at different severity levels (Kaiser 2020 and Heidarzadeh et al. 2021). In underground tunnels, stability is greatly influenced by the quality of rock and the variabilities associated with estimation / measurement of in-situ stress state. At shallow depths, blocky to disintegrated rock masses (moderate quality) fail under structurally controlled gravity-driven modes such as gravity falling or sliding of wedges. By increasing depth, hence the magnitude of in-situ stresses, the dominant mode of failure shifts to a combination of structurally controlled and stress-assisted (or stress-driven), i.e., localized brittle failure of intact rock with the unraveling of rock blocks. Ultimately, under high in-situ stresses, a jointed rock mass may behave as a massive rock, hence brittle failure occurs around the entire excavation area (Villaescusa 2014 and Kaiser 2020). Understanding the level of damage within the rock mass is crucial for modifying and adjusting ground support. Fragility curves and vulnerability functions developed through probabilistic numerical analysis can aid in this assessment. While fragility curves have traditionally been used to evaluate seismic vulnerability, this study aims to

introduce a methodology for assessing the robustness of underground tunnels against brittle modes of failure based on rock mass quality and static loading intensities.

2 FRAGILITY CURVES AND VULNERABILITY FUNCTIONS

The fragility of an underground tunnel can be assessed by a mathematical function that relates the probability of reaching a certain damage state (DSi) to a specific static loading intensity measure. This function can be expressed as a log-normal cumulative probability density function, shown in Equation 1 (Saeidi et al. 2019).

$$P[Damage \geq DS_i(I)] = \int_0^I \frac{1}{I\sigma\sqrt{\pi}} \exp\left[\frac{-1}{2}\left(\frac{\ln(I)-\mu}{\sigma}\right)^2\right] dI \quad (1)$$

where P [Damage ≥ DSi(I)] represents the probability that a damage level reaches or exceeds a certain damage state threshold (DSi), μ and σ are the mean and standard deviation values of ln(*I*), respectively, and *I* denotes the loading intensity factor. Furthermore, the probability function presented in Equation 1 can also be expressed as Equations 2 and 3.

$$P[Damage \geq DS_i(I)] = 1 - P[Damage < DS_i] \quad (2)$$

$$P[Damage < DS_i] = \sum_{j=1}^{i-1} \frac{N(DS_i)}{n} = \sum_{j=1}^{i-1} P(DS_j) \quad (3)$$

where P(DSj) is the probability of failure for rock damage class DSj (Saeidi et al. 2019).

3 THE PROBABILISTIC METHODOLOGY

The study began by probabilistically determining geomechanical parameters for three rock mass quality classes and estimating in-situ stress as a function of depth. A static loading intensity measure was then calculated using the principal components of in-situ stress for each depth. Numerical analyses were conducted using FLAC3D and the brittle shear ratio (BSR) failure criterion. Probability of occurrence was calculated for each damage state, and fragility curves and vulnerability functions were developed to assess the impact of static loading intensity and rock mass quality on tunnel stability.

3.1 Probabilistic determination of rock mass geomechanical parameters

The moderate quality blocky rock mass was categorized into three classes based on the geological strength index (GSI) values (30–50, 50–60, and 60–70). Mean and standard deviation values were assigned to GSI, intact uniaxial compressive strength (UCS), the Hoek–Brown material constant (m_i), Young's modulus (E_i), and Poisson's ratio (υ) for each class (Table 1). The values were selected based on data obtained from various underground mining and civil projects in Canada.

Table 1. The selected range, mean and standard deviation (s.d.) of the input parameters.

Parameter	Minimum–Maximum	Mean (s.d.)	Parameter	Minimum–Maximum	Mean (s.d.)
σ_{ci} (MPa)	30.3–204	111.0 (35.5)	m_i	4.5–22	13.0 (3.8)
GSI (I)	30–50	40.0 (4.4)	E_i (GPa)	20.7–91.4	61.4 (17.2)
GSI (II)	50–60	55.0 (1.9)	υ	0.11–0.39	0.26 (0.06)
GSI (III)	60–70	65.0 (1.9)			

To estimate the strength and deformability parameters of each rock mass class, we utilized the Monte Carlo Simulation (MCS) method with 10000 iterations. We assigned a normal probability distribution function (PDF) to all the input parameters, as mentioned earlier, and applied equations provided by Hoek (2007). The resulting values are presented in Table 2.

Table 2. The mean, s.d., minimum, maximum, and best-fitted PDFs of the rock mass parameters.

Class	Parameter	PDF	Mean	s.d.	Minimum
	m_b	Beta-General	1.57	0.58	0.32
	S	Beta-General	0.0014	0.0004	0.0004
GSI (I)	a	Beta-General	0.51	0.003	0.505
	m_b	Kumaraswamy	2.62	0.79	0.75
	S	Beta-General	0.0069	0.0014	0.0035
GSI (II)	a	Beta-General	0.504	0.0005	0.502
	m_b	Kumaraswamy	3.75	1.14	1.06
	S	Beta-General	0.02	0.004	0.01
GSI (III)	a	Beta-General	0.502	0.0003	0.501

3.2 Determining the state of in-situ stress

To estimate the in-situ stress state, the Canadian Shield was used as a reference, and the in-situ stress components were calculated as a function of depth using the formula of Young & Maloney (2015). Equations 4 to 6 provide the relevant equations for this estimation process.

$$\sigma_1\ [\text{MPa}] = (0.040 \pm 0.001) \times z\ [\text{m}] - (9.185 \pm 1.500) \quad (4)$$

$$\sigma_2\ [\text{MPa}] = (0.029 \pm 0.001) \times z\ [\text{m}] + (4.617 \pm 1.159) \quad (5)$$

$$\sigma_3\ [\text{MPa}] = (0.021 \pm 0.001) \times z\ [\text{m}] - (0.777 \pm 0.872) \quad (6)$$

The maximum principal stress component is applied horizontally and perpendicular to the strike of the tunnel, and the minimum principal stress component is assumed to be applied vertically.

3.3 Defining the measure of static loading intensity

In this study, we defined a loading demand parameter to provide an intensity measure for the static loading around the tunnel. The defined static loading intensity measure (SLIM) is formulated in Equation 7.

$$SLIM = \sigma_1 / (\sigma_1 - \sigma_3) \quad (7)$$

where σ_1 and σ_3 are the major and minor principal in-situ stress components respectively. The selected tunnel depths and their associated *SLIMs* used in this study are presented in Table 3.

Table 3. The principal stress components and intensity measures with tunnel depth.

Tunnel depth (m)	σ_1 (MPa)	σ_2 (MPa)	σ_3 (MPa)	*SLIM*	Stress condition
55	8.41	5.40	0.38	1.0	Low in-situ stress ($\sigma_1/\sigma_c < 0.15$)
115	10.70	6.53	1.64	1.2	
195	13.73	8.05	3.32	1.3	

295	17.53	9.95	5.42	1.4	Intermediate in-situ stress ($0.15 < \sigma_1/\sigma_c < 0.4$)
595	33.66	23.27	11.72	1.5	
735	38.98	26.63	14.66	1.6	
955	47.34	31.91	19.28	1.7	High in-situ stress ($\sigma_1/\sigma_c > 0.4$)
1355	62.54	41.51	27.68	1.8	
3055	127.14	82.31	63.38	2.0	

3.4 Selection of the failure criteria

The brittle shear ratio (BSR) was chosen to evaluate the level of damage in the surrounding brittle rock mass of an underground tunnel. BSR is a differential stress-based criterion and has been used in previous studies (Castro et al. 2012). BSR is calculated via Equation 8, and the resulting values are categorized in Table 4 to indicate rock mass brittle damage intensity.

$$BSR = \frac{(\sigma_1 - \sigma_3)}{UCS_{intact}} \tag{8}$$

Table 4. The level of rock damage in relation to the BSR (adapted from Castro et al. 2012).

Damage State	$(\sigma_1 - \sigma_3)$/UCS	Damage intensity.	Strainburst potential
ND	0.35	No to minor	No
1	0.35–0.45	Minor (spalling)	No
2	0.45–0.6	Moderate (breakout formation)	Minor
3	0.6–0.7	Moderate to major	Moderate
4	> 0.7	Major	Major

3.5 Numerical modeling

Each FLAC3D model featured an identical 6 × 5 × 25 m horseshoe-shaped tunnel geometry within the rock mass. A finer mesh size was employed near the tunnel periphery for improved accuracy. External boundary roller conditions were positioned away from the region of interest to avoid negative impacts. The tunnel was excavated in one step, allowing equilibrium to be reached afterwards.

4 RESULTS AND DISCUSSION

We evaluated the level of brittle damage for each simulation model by plotting BSR contours and identifying the zone with the highest BSR value (Figure 1). We calculated the probability of damage occurrence as the ratio of the number of model simulations showing the maximum damage level for a specific damage state to the total number of simulations for each *SLIM* group.

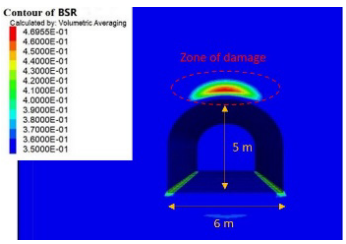

Figure 1. An example of the resulting contours for BSR.

Table 5 presents the BSR fragility curves and the mean damage method parameters μ and σ for each rock mass class. Figure 2 displays four vulnerability functions (DS1, DS2, DS3, and DS4) for each

class, obtained by substituting the values of μ and σ into Equation 1. Nonlinear regression analysis determined these values. The fragility curves and their corresponding vulnerability functions were employed to assess brittle damage or failure around the tunnel in the three rock mass classes.

Table 5. The values of μ and σ of BSR for the rock mass quality classes. (DS1: Minor damage − spalling; DS2: Moderate damage − breakout formation; DS3: Moderate to major; DS4: Major damage)

Rock mass class	DS1		DS2		DS3		DS4	
	μ	σ	μ	σ	μ	σ	μ	σ
GSI 30–50	0.388	0.043	0.437	0.060	0.523	0.088	0.600	0.110
GSI 50–60	0.387	0.036	0.427	0.056	0.515	0.098	0.575	0.113
GSI 60–70	0.389	0.037	0.426	0.056	0.533	0.095	0.562	0.112

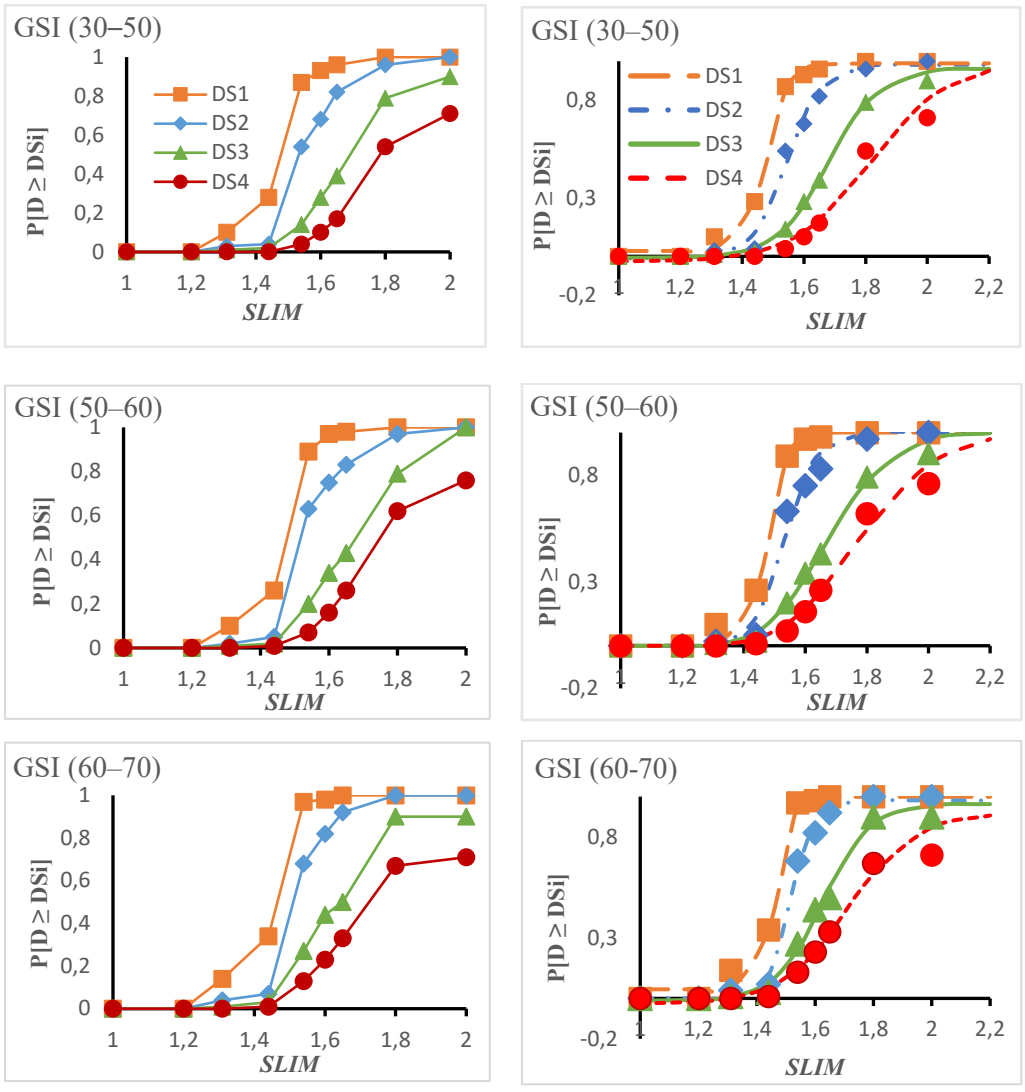

Figure 2. The BSR fragility curves and vulnerability functions for each rock mass quality class.

The fragility curves for the three rock mass quality classes exhibit similar patterns, as shown in Figure 2. DS1 has the highest probability of occurrence across all rock mass quality classes, followed by DS2, DS3, and DS4. Additionally, PDSi is generally higher in weaker rock masses and lower in stronger ones, for all damage states. In low-stress environments with SLIMs between 1.0 and 1.3, the mechanism of failure around the tunnel is mainly structurally controlled, and the probabilities of

damage states caused by stress-induced mechanisms are low. The highest probability of occurrence for stress-induced damage is 14% for the GSI class of 60-70 at a SLIM of 1.3. As the SLIM increases from 1.4 to 1.6, the mechanism of failure shifts to a combination of structurally controlled and stress assisted. The spalling limit is calculated to be between a SLIM of 1.4 and 1.5 for stress-assisted damage, which marks the boundary between inner and outer shell damage around the tunnel periphery. Between SLIM values of 1.0 to 1.44, where the confinement is still low, PDS1 (probability of minor spalling) increases to values over 25% for all three rock mass quality classes, while the probabilities of higher damage states (PDS2, PDS3, and PDS4) are negligible, less than 5%. As SLIM values increase between 1.44 and 1.54, there is a significant increase in PDS1, exceeding 90% for all three rock mass quality classes, indicating a transition from inner to outer shell damage around the tunnel. The probability of moderate damage (PDS2) exceeds 50% for all rock mass quality classes, while the probabilities of moderate to major damage (PDS3) and major damage (PDS4) also increase to 27% and 13%, respectively. This suggests that extensive stress-induced damage of intact rock occurs around the tunnel under such circumstances. The probability of damage states PDS1 and PDS2 increases to 100% and 95%, respectively, for the three rock mass quality classes as the SLIM exceeds 1.8. PDS3 and PDS4 also reach values greater than 80% and 55%, respectively. This indicates severe rock mass damage around the tunnel and extensive brittle failure of the intact rock. At SLIM values of 2, which corresponds to depths greater than 3000 m, PDS1 and PDS2 reach 100%, and PDS3 and PDS4 exceed 90% and 70%, respectively, for all three rock mass classes. Under such conditions, the outer shell shear rupture (failure) of intact rock is likely to occur around the tunnel. Our study aimed to confirm if the behavior observed in simulations with the same SLIM but different in situ stress magnitudes is consistent. Our verification analyses showed that the BSR values within a distance equal to the tunnel radius (2.5 m) are nearly identical among models with varying stress states, indicating that our defined SLIM is independent of stress estimation approaches.

5 CONCLUSION

We proposed a methodology for assessing the stability of underground tunnels by creating fragility curves that considered variations in rock mass quality and static loading. It was found that the BSR fragility curves were able to explain the evolution of damage in the inner and outer shell stress spaces for the three rock mass quality classes. It was also verified that the fragility curves could be used in other similar cases to predict levels of different damage states around a tunnel, while considering variations in rock mass quality and static loading intensity.

REFERENCES

Castro, L. A. M., Bewick, R. P., & Carter, T. G. (2012). An overview of numerical modelling applied to deep mining. In R. Azevedo (Ed.), *Innovative numerical modelling in geomechanics* (pp. 393–414). CRC Press — Taylor & Francis Group.

Heidarzadeh, S., Saeidi, A., & Rouleau, A. (2021). The damage-failure criteria for numerical stability analysis of underground excavations: A review. *TUST, 107*, 103633, ISSN 0886-7798.

Hoek, E. (2007). Practical rock engineering. http://www.rocscience.com/hoek/PracticalRockEngineering.

Kaiser, P. K. (2020). From common to best practices in underground rock engineering. In: S.A.B. da Fontoura, R.J. Rocca & J. Pavon Mendoza (eds). *Rock mechanics for natural resources and infrastructure development*. Taylor & Francis Group, London. pp. 141–182.

Saeidi, A. Eslami, E. Quirion, M. Seifaddini, M. (2019). Assessment of rock mass erosion in unlined spillways using developed vulnerability and fragility functions, *Georisk: Assessment and Management of Risk for Engineered Systems and Geohazards*, *14(4)*, 280–292. DOI: 0.1080/17499518.2019.1660796.

Villaescusa, E. (2014). Geotechnical design for sublevel open stoping. CRC Press. https://doi.org/10.1201/b16702.

Young, S., Maloney, S. (2015). An Update to the Canadian Shield Stress Database. MIRARCO. NWMO-TR-2015-18.